Fabrication of Titanium Dioxide Thin Flakes and Their Porous Aggregate

Takayoshi Sasaki,*,† Satoshi Nakano,† Shoichi Yamauchi,‡ and Mamoru Watanabe†

National Institute for Research in Inorganic Materials, 1-1 Namiki, Tsukuba, Ibaraki 305, Japan, and Tosoh Corporation, 43 Miyukigaoka, Tsukuba, Ibaraki 305, Japan

Received August 12, 1996. Revised Manuscript Received October 14, 1996[⊗]

Thin flakes of titanium dioxide have been synthesized through a novel route via exfoliation of a layered precursor. A protonic oxide of $H_xTi_{2-x/4}\square_{x/4}O_4 \cdot H_2O$ ($x \sim 0.7$; □, vacancy) was delaminated into colloidal single sheets (thickness 0.75 nm) by being interacted with a bulky organic amine, $(C_4H_9)_4NOH$. The resulting titania sol was freeze-dried to produce a gel in a thin filmlike texture. The gelation took place by reassembling 10−20 titanate sheets and consequently yielding lamellar aggregates. Upon heating above 400 °C, the gel was transformed into titanium dioxide (anatase) in thin flaky morphology (20−30 nm in thickness versus ~μm in the lateral dimension). Intermediates at various stages of the synthetic process as well as the final product were examined by applying various characterization techniques such as X-ray diffraction (XRD), scanning and transmission electron microscopes (SEM, TEM), FT-IR and Raman spectroscopies, thermogravimetry, and elemental analysis. The flaky particulates were aggregated in a disordered fashion to make an open microstructure. Nitrogen gas physisorption measurements revealed that the material was meso- to macroporous having a BET surface area of 40−110 $m^2\ g^{-1}$. Photocatalytic activity for the material was demonstrated for a degradation reaction of aqueous trichloroethylene.

Introduction

Titanium dioxide is one of the most important oxides, attracting much attention from both fundamental and practical viewpoints. Its photocatalytic properties have been investigated extensively; UV−visible light irradiation induces effective charge separation into electrons and holes. Their redox potential is powerful enough to cleave H_2O into H_2 and O_2 gas, and decompose hazardous pollutants into innocuous substances,[1,2] which is a promising prospect as sources of clean energy and solution of environmental problems. Furthermore, titanium dioxide powders have a number of industrial applications as pigments, cosmetics, and so on, which is owing to their versatility in connection with high chemical stability, tinting strength, hiding power, and UV ray shielding capability.[3,4]

The titanium dioxides of various nature have been synthesized to optimize them toward a particular purpose. One of such efforts has been devoted to preparation of ultrafine powdery materials.[5,6] The particle size is controlled down to the order of tens of nanometers, which results in reduction of visible light scattering and enhancement of catalytic activities. The size quantization effect reported for the nanoparticle oxide has also stimulated fundamental interest.[6]

In contrast to size control, shape control of particulates, especially thinner ones in a nanometer scale, is more difficult and challenging topic. Most of the fine powders synthesized so far possess virtually spherical forms. Thin films and fibers have been synthesized mostly by being supported on the surface of substrates or in the interstices in some three-dimensional networks.[7,8] If self-standing flakes or fibers can be obtained, novel properties may be expected.

There are a number of layered compounds which undergo intercalation reactions incorporating various guests into their galleries.[9] Normal intercalation reactions bring about intersheet expansion in accordance with guest dimensions. Recently the swelling to infinity, in other words, delamination into single sheets, has been reported in the case of particular guests for several classes of layered materials, e.g., smectite clay minerals,[10] zirconium phosphates,[11] transition-metal chalcogenides,[12] and layered perovskites.[13] Colloidal single-sheet suspensions of these compounds may be used as

† National Institute for Research in Inorganic Materials.
‡ Tosoh Corp.
[⊗] Abstract published in *Advance ACS Abstracts,* December 1, 1996.

(1) (a) Fujishima, A.; Honda, K. *Nature* **1972**, *238*, 37. (b) Frank, S. N.; Bard, A. J. *J. Phys. Chem.* **1977**, *81*, 1484.
(2) Wold, A. *Chem. Mater.* **1993**, *5*, 280.
(3) Clark, R. J. H. *Comprehensive Inorganic Chemistry*; *Vol. 3*, Bailar, J. C., Emeleus, H. J., Nyholm, S. R., Eds.; Pergamon Press: New York, 1973; pp 375−77.
(4) Kirk, R. E.; Othmer, D. F. *Encyclopedia of Chemical Technology*; Mark, H. F., Othmer, D. F., Overberger, C. G., Seaborg, G. T., Eds.; John Wiley and Sons: New York, 1982; p 803.
(5) Henglein, A. *Chem. Rev.* **1989**, *89*, 1861.
(6) (a) Anpo, M.; Shima, T.; Kodama, S.; Kubokawa, Y. *J. Phys. Chem.* **1987**, *91*, 4305. (b) Kormann, C.; Bahnemann, D. W.; Hofmann, M. R. *J. Phys. Chem.* **1988**, *92*, 5196. (c) Serpone, N.; Lawless, D.; Khairutdinov, R. *J. Phys. Chem.* **1995**, *99*, 16646.
(7) *Sol-Gel Technology for Thin Films, Fibers, Performs, Electronics and Specialty Shapes*; Klein, L. C., Ed.; Noyes Publication: Park Ridge, NJ, 1988.
(8) Anpo, M.; Aikawa, N.; Kubokawa, Y.; Che, M.; Louis, C.; Giamello, E. *J. Phys. Chem.* **1985**, *89*, 5017.
(9) *Intercalation Chemistry*; Whittingham, M. S., Jacobson, A. J., Eds.; Academic Press: New York, 1982.
(10) (a) Nadeau, P. H.; Wilson, M. J.; McHardy, W. J.; Tait, J. M. *Science* **1984**, *225*, 923. (b) Nadeau, P. H.; Tait, J. M.; McHardy, W. J.; Wilson, M. J. *Clay Miner.* **1984**, *19*, 67. (c) Nadeau, P. H.; Wilson, M. J.; McHardy, W. J.; Tait, J. M. *Clay Miner.* **1984**, *19*, 757.
(11) Alberti, G.; Casciola, M.; Costantino, U. *J. Colloid Interface Sci.* **1985**, *107*, 256.

S0897-4756(96)00432-2 CCC: $14.00

sources for syntheses of novel materials. Some examples have been demonstrated in preparations of nanocomposites of organic polymers−inorganic layered hosts,[14] self-assembled multilayer films,[15] and microporous materials with inorganic pillars.[16]

In addition to the material designs above, we anticipate that very thin flakes may be derived from the delaminated layered materials. Four types of layered protonic titanates such as $H_2Ti_3O_7$,[17] $H_2Ti_4O_9{\cdot}1.2H_2O$,[18] $H_2Ti_5O_{11}{\cdot}3H_2O$[19] and $H_xTi_{2-x/4}\square_{x/4}O_4{\cdot}H_2O$ ($x \sim 0.7$; □, vacancy)[20] have been synthesized by acid exchange of corresponding alkali-metal titanates. The compounds exhibit Brønsted acidity intercalating a variety of cations and organic amines.[18b,19,20b,21−27] We have demonstrated that $H_xTi_{2-x/4}\square_{x/4}O_4{\cdot}H_2O$ undergoes exfoliation on the action of bulky amines.[28] The present paper describes the synthesis of very thin flakes of titanium dioxide and their porous assemblage, which are derived from the colloidal single sheets of the titanate.

Experimental Section

Reagents and Materials. The starting material, $H_xTi_{2-x/4}\square_{x/4}O_4{\cdot}H_2O$ ($x = 0.70$), was prepared from $Cs_xTi_{2-x/4}\square_{x/4}O_4$ by acid exchange as previously described.[20] Solid-state calcination of Cs_2CO_3 and TiO_2 (1:2.65 in molar ratio) at 800 °C produced a polycrystalline powder of $Cs_xTi_{2-x/4}\square_{x/4}O_4$.[20,29] The reagents used were of 99.99% purity (Rare Metallic, Co.). The Cs titanate was converted into the protonic form by being stirred in a HCl solution (1 mol dm^{-3}) at ambient temperature. After four cycles of acid exchange, the sample was filtered and washed with a copious amount of water to eliminate excess acid. The product was air-dried and stored in a desiccator at a relative humidity of 70%.

Preparation of Colloidal Single-Sheet Suspensions. A weighed amount of $H_xTi_{2-x/4}\square_{x/4}O_4{\cdot}H_2O$ was interacted with an aqueous solution of tetrabutylammonium hydroxide $(C_4H_9)_4NOH$ (abbreviated as TBAOH hereafter). TBAOH was of analytical grade and used as received from Aldrich, Co. Milli-Q filtered water (Millipore, Co.; >15 MΩ cm^{-1}) was used in all preparations. The mixture was shaken vigorously (180 rpm) at 25 ± 0.5 °C for 10 days, which produced an opalescent suspension. A typical composition of the sol was 0.4 wt % and dose of TBAOH was adjusted to 5-fold excess to the molar equivalent of the exchangeable protons in $H_xTi_{2-x/4}\square_{x/4}O_4{\cdot}H_2O$.

X-ray Diffraction. Powder XRD data were collected on a Rigaku Rint-2000 diffractometer with a graphite-monochromatized Cu Kα radiation (λ = 0.154 05 nm). A horizontal goniometer in a humidity-controllable chamber (relative humidity 5−95%) makes measurements on fluid samples such as colloidal suspensions possible.

The crystallite size, t, was calculated by the Sherrer equation:[30]

$$t = k\lambda/(\beta_{cryst}\cos\theta) \quad (1)$$

where β_{cryst} and θ are intrinsic line breadth (fwhm) arising from crystallite size and the Bragg angle of the diffraction peak, respectively. The shape constant, k, was set to 0.9, which is recommended in most cases. Measured line width, β_{obs}, should be corrected in terms of instrumental broadening, β_{instr}. By assuming the Warren's relation[30] below, the instrumental broadening was negligible in the present case:

$$\beta_{obs}^2 = \beta_{cryst}^2 + \beta_{instr}^2 \quad (2)$$

The instrumental resolution experimentally determined was 0.09° for 2θ < 15° (using $CH_2(CH_2)_{12}CH_2OH$ as reference material) and 0.12° for 2θ > 25° (α-SiO_2) while the observed breadth was much larger, in the range 0.5°.

Electron Microscopy. Morphological changes of the material were followed by a Hitachi S-5000 scanning electron microscope equipped with a field emission gun. The starting material, $H_xTi_{2-x/4}\square_{x/4}O_4{\cdot}H_2O$, was coated with Pt by a conventional deposition technique while samples in the flaky texture were coated by Os vapor deposition (Nippon Laser & Electronics Lab.; NL-OP50-FS) to prevent charge buildup effectively. Transmission electron micrographs were obtained using a JEOL H-500 apparatus operated at an accelerating voltage of 100 kV. Samples were dispersed in CCl_4 ultrasonically and supported onto a carbon-coated Cu grids.

Vibrational Spectroscopy. Infrared spectra were recorded on a sample pressed into a KBr disk by using a Digilab S-45 FT-IR spectrophotometer in the range of 400−4000 cm^{-1} with a resolution of 2 cm^{-1}. Raman spectra were acquired in backscattering geometry by exciting a sample on a slide glass with an Ar^+ laser of 514.5 nm (Jobin Yvon T-64000). A spectral resolution was 2 cm^{-1}.

Thermal Analysis. Thermogravimetric measurements were performed in air at a heating rate of 10 °C min^{-1} using a Rigaku TAS 200 thermal analyzer.

Elemental Analysis.[31] Organic components in the freeze-dried gel were determined by a Perkin-Elmer 2400-type CHNS/O analyzer. The Ti content was obtained gravimetrically as TiO_2. A weighed amount of the gel was decomposed

(12) (a) Liu, C.; Singh, O.; Joensen, P.; Curzon, A. E.; Frindt, R. F. *Thin Solid Films* **1984**, *113*, 165. (b) Joensen, P.; Frindt, R. F.; Morrison, S. R. *Mater. Res. Bull.* **1986**, *21*, 457. (c) Joensen, P.; Crozier, E. D.; Alberding, N.; Frindt, R. F. *J. Phys. C.: Solid State Phys.* **1987**, *20*, 4043. (d) Yang, D.; Jiménez Sandoval, S.; Divigalpitiya, W. M. R.; Irwin, J. C.; Frindt, R. F. *Phys. Rev. B* **1991**, *43*, 12053.

(13) Treacy, M. M. J.; Rice, S. B.; Jacobson, A. J.; Lewandowski, J. T. *Chem. Mater.* **1990**, *2*, 279.

(14) (a) Kanatzidis, M. G.; Bissessur, R.; DeGroot, D. C.; Schindler, J. L.; Kannewurf, C. R. *Chem. Mater.* **1993**, *5*, 595. (b) Wu, J.; Lerner, M. M. *Chem. Mater.* **1993**, *5*, 835. (c) Lemmon, J. P.; Lerner, M. M. *Chem. Mater.* **1994**, *6*, 207.

(15) (a) Kleinfeld, E. R.; Ferguson, G. S. *Science* **1994**, *265*, 370. (b) Keller, S. W.; Kim, H.-N.; Mallouk, T. E. *J. Am. Chem. Soc.* **1994**, *116*, 8817.

(16) Nazar, L. F.; Liblong, S. W.; Yin, X. T. *J. Am. Chem. Soc.* **1991**, *113*, 5889.

(17) (a) Izawa, H.; Kikkawa, S.; Koizumi, M. *J. Phys. Chem.* **1982**, *86*, 5023. (b) Feist, T. P.; Mocarski, S. J.; Davies, P. K.; Jacobson, A. J.; Lewandowski, J. T. *Solid State Ionics* **1988**, *28*−30, 1338. (c) Feist, T. P.; Davies, P. K. *J. Solid State Chem.* **1992**, *101*, 275.

(18) (a) Marchand, R.; Brohan, L.; Tournoux, M. *Mater. Res. Bull.* **1980**, *15*, 1129. (b) Sasaki, T.; Watanabe, M.; Komatsu, Y.; Fujiki, Y. *Inorg. Chem.* **1985**, *24*, 2265.

(19) Sasaki, T.; Komatsu, Y.; Fujiki, Y. *Chem. Mater.* **1992**, *4*, 894.

(20) (a) Sasaki, T.; Komatsu, Y.; Fujiki, Y. *J. Chem. Soc., Chem. Commun.* **1991**, 817. (b) Sasaki, T.; Watanabe, M.; Michiue, Y.; Komatsu, Y.; Izumi, F.; Takenouchi, S. *Chem. Mater.* **1995**, *7*, 1001.

(21) (a) Izawa, H.; Kikkawa, S.; Koizumi, M. *J. Solid State Chem.* **1985**, *60*, 264. (b) Izawa, H.; Kikkawa, S.; Koizumi, M. *J. Solid State Chem.* **1987**, *69*, 336.

(22) (a) Sasaki, T.; Watanabe, M.; Komatsu, Y.; Fujiki, Y. *Bull. Chem. Soc. Jpn.* **1985**, *58*, 3500. (c) Sasaki, T.; Komatsu, Y.; Fujiki, Y. *Mater. Res. Bull.* **1987**, *22*, 1321. (d) Sasaki, T.; Komatsu, Y.; Fujiki, Y. *Inorg. Chem.* **1989**, *28*, 2776.

(23) Izawa, H.; Kikkawa, S.; Koizumi, M. *Polyhedron* **1983**, *2*, 741.

(24) (a) Clément, P.; Marchand, R. *C. R. Acad. Sci. Paris Ser. II* **1983**, *296*, 1161. (b) Miyata, H.; Sugahara, Y.; Kuroda, K.; Kato, C. *J. Chem. Soc., Faraday Trans. 1* **1988**, *84*, 2677.

(25) Sasaki, T.; Izumi, F.; Watanabe, M. *Chem. Mater.* **1996**, *8*, 777.

(26) (a) Anderson, M. W.; Klinowski, J. *Inorg. Chem.* **1990**, *29*, 3260. (b) Landis, M. E.; Aufdembrink, B. A.; Chu, P.; Johnson, I. D.; Kirker, G. W.; Rubin, M. K. *J. Am. Chem. Soc.* **1991**, *113*, 3189.

(27) (a) Cheng, S.; Wang, T.-C. *Inorg. Chem.* **1989**, *28*, 1283. (b) Sylvester, P.; Cahill, R.; Clearfield, A. *Chem. Mater.* **1994**, *6*, 1890. (c) Hou, W.; Yan, Q.; Peng, B.; Fu, X. *J. Mater. Chem.* **1995**, *5*, 109.

(28) (a) Sasaki, T.; Watanabe, M.; Hashizume, H.; Yamada, H.; Nakazawa, H. *J. Chem. Soc., Chem. Commun.* **1996**, 229. (b) Sasaki, T.; Watanabe, M.; Hashizume, H.; Yamada, H.; Nakazawa, H. *J. Am. Chem. Soc.* **1996**, *118*, 8329.

(29) (a) Hervieu, M.; Raveau, B. *Rev. Chim. Min.* **1981**, *18*, 642. (b) Grey, I. E.; Madsen, I. C.; Watts, J. A.; Bursill, L. A.; Kwiatkowska, J. *J. Solid State Chem.* **1985**, *58*, 350. (c) Grey, I. E.; Li, C.; Madsen, I. C.; Watts, J. A. *J. Solid State Chem.* **1987**, *66*, 7.

(30) Cullity, B. D., *Elements of X-ray Diffraction*; Addison-Wesley: Reading, MA, 1957.

(31) Sumika Analytical Laboratory, Niihama, Ehime 792, Japan.

(32) Dollimore, D.; Heal, G. R. *J. Appl. Chem.* **1964**, *14*, 109.

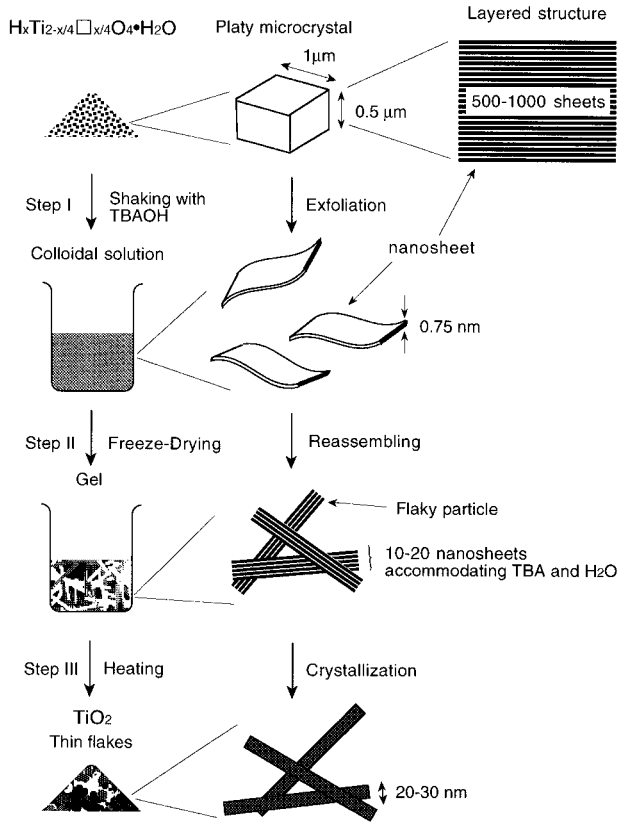

Figure 1. Schematic illustration of synthetic process of the titanium dioxide thin flakes.

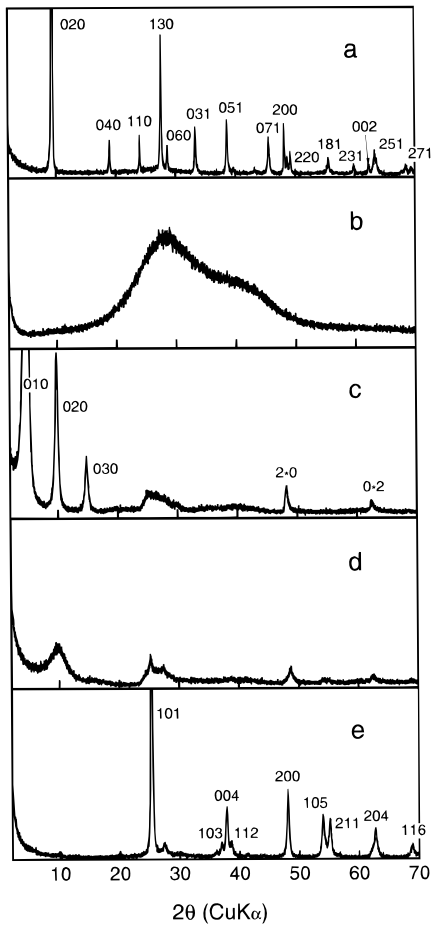

Figure 2. XRD profiles at various stages of the synthetic process. (a) starting material, $H_xTi_{2-x/4}\square_{x/4}O_4\cdot H_2O$, (b) colloidal suspension (recorded as is), (c) freeze-dried product of the suspension, (d) titanium dioxide thin flakes heat-treated at 350 °C for 1 h, (e) the material prepared at 700 °C. Indexes given in (a), (c), and (e) are based on the orthorhombic layered structure for $H_xTi_{2-x/4}\square_{x/4}O_4\cdot H_2O$, the turbostratic lamellar structure for the TBA-intercalated titanate and anatase, respectively.

with a H_2SO_4 solution, from which a Ti cupfferon complex was precipitated. The complex was calcined to TiO_2 to be weighed.

Nitrogen Gas Adsorption/Desorption Measurement. A Nippon Bell Belsorp 36 instrument was employed to obtain adsorption/desorption isotherms at −196 °C. A sample (∼0.3 g) was outgassed under vacuum for 2 h at 200 °C prior to each measurement. The specific surface area was calculated in a relative pressure range of $0.05 < P/P_0 < 0.2$. The pore-size distribution was obtained from the adsorption branches based on the method of Dollimore and Heal.[32]

Measurement of Photocatalytic Activity. Catalytic properties of the titanium dioxide thin flakes were evaluated by examining photodecomposition reaction of a typical halocarbon, trichloroethylene, $ClCH{=}CCl_2$. A weighed amount of the sample (0.1 g) was dispersed in a 100 cm^3 of trichloroethylene aqueous solution. The concentration and pH value of the solution was 10 ppm and ∼5, respectively. The closed system was irradiated by UV light (15 W, 354 nm) at room temperature, and a change in concentration of the reactant was monitored by gas chromatography (JEOL GC-311).

Results and Discussion

Synthetic Process. Figure 1 illustrates the synthetic route, which consists of three steps. XRD, SEM, and Raman data at various stages of the process are shown in Figures 2−4. The starting protonic oxide, $H_xTi_{2-x/4}\square_{x/4}O_4\cdot H_2O$, was composed of micrometer-sized platy crystallites (Figure 3a). The dimensions indicate that one microcrystal comprises several hundreds of the host sheets depicted in Figure 5. The essential step of this synthetic approach is the delamination of the layered precursor compound (step I). The action of bulky organic bases such as TBAOH produced the stable colloidal suspension. It has been demonstrated that the layered structure is completely separated into single sheets which are 0.75 nm thick.[28] Note the change in XRD data from the pattern with sharp lines to the amorphous halo one (see Figure 2a,b). The amorphous halo is attributed to scattering from dispersed single sheets of the titanate and water as a solvent. It is to be pointed out that a titanate−water mixture at this concentration (0.4 wt %) should produce well-detectable diffraction if the titanate is not delaminated.

Freeze-drying of the colloidal suspension (step II) yielded a voluminous white solid with cotton-like appearance. SEM observation demonstrated that the parent microcrystals were broken down to flaky particulates which were thin enough to be flexible (Figure 3b). A set of sharp diffraction lines appeared again in a low angular range (see Figure 2c). These reflections can be indexed as $0k0$ (k = 1, 2, 3), which is indicative of a lamellar structure with a gallery height of 1.75 nm. Absence of *hkl* reflections as well as asymmetric line profiles for $2{*}0$ and $0{*}2$ diffraction bands revealed the turbostratic nature of the structure. The coherent interference length was calculated to be ∼25 nm from the line breadth of the $0k0$ series. This value agrees roughly with the thickness of the thin flakes (20−30 nm) in the micrograph (Figure 3d). These results lead to the conclusion that 10−20 titanate sheets were restacked upon freeze drying, resulting in a TBA-intercalated compound.

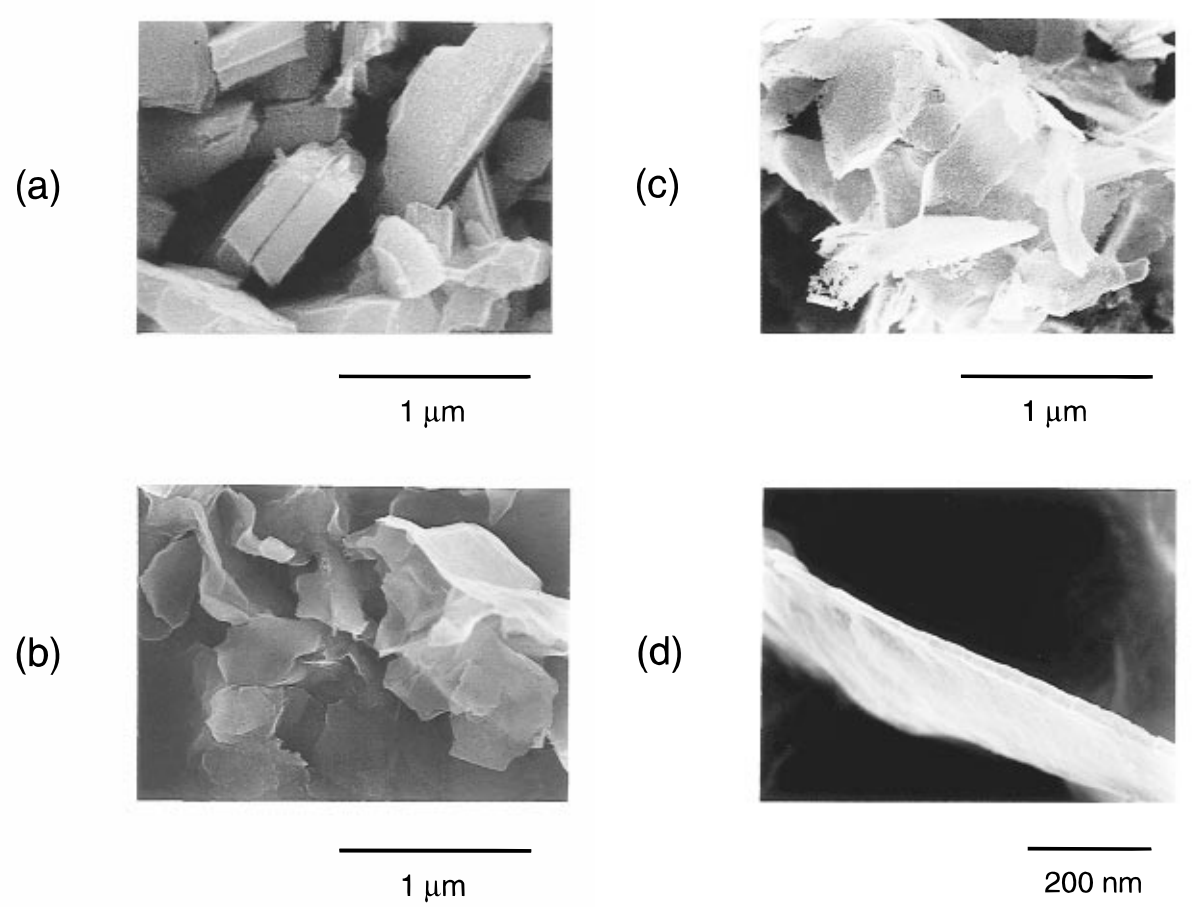

Figure 3. Scanning electron micrographs: (a) $H_xTi_{2-x/4}\square_{x/4}O_4 \cdot H_2O$, (b) freeze-dried gel, (c) thin flakes of titanium dioxide heat-treated at 700 °C, and (d) edge view of the flake. Dots on the surface of the crystals of $H_xTi_{2-x/4}\square_{x/4}O_4 \cdot H_2O$ are Pt grains deposited.

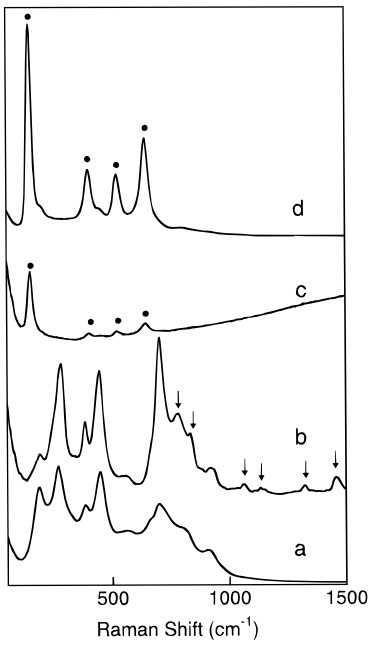

Figure 4. Raman spectra: (a) $H_xTi_{2-x/4}\square_{x/4}O_4 \cdot H_2O$, (b) freeze-dried product, (c) titanium dioxide thin flakes heat-treated at 350 °C, and (d) the material prepared at 700 °C. Peaks designated by circles and arrows are assignable to anatase and TBA, respectively.

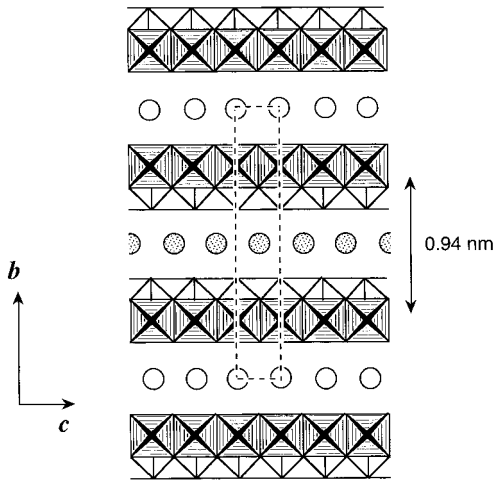

Figure 5. Polyhedral representation of crystal structure for the layered protonic oxide $H_xTi_{2-x/4}\square_{x/4}O_4 \cdot H_2O$. TiO_6 octahedra are combined with each other via edge-sharing to produce a lepidocrocite (FeOOH)-type two-dimensional sheet. The host sheets are stacked in a body-centered orthorhombic relationship, accommodating H_2O (designated as circles) between them. Broken lines encircle the unit cell, the dimensions of which are $a = 0.3783(2)$ nm, $b = 1.8735(8)$ nm, and $c = 0.2978(2)$ nm for $x = 0.7$.[20] Approximately 70% of the interlayer H_2O molecules are protonated to H_3O^+ ions. The positive charge is balanced with minus one of the host sheets arising from the Ti site vacancies.

The composition of the gel was determined to be $((C_4H_9)_4N)_{0.3}H_{0.7}Ti_{1.825}\square_{0.175}O_4 \cdot 0.7H_2O$ (Calcd: Ti, 36.8%; C, 24.3%; H, 5.5%; N, 1.8%. Found: Ti, 36.5%; C, 24.5%; H, 5.1%; N, 1.6%).[31] Vibrational spectra confirmed that TBA ions and H_2O species were trapped in the lattice. The broad infrared bands centered at 3440 and 1627 cm^{-1} are attributable to stretching and bending modes for H_2O, respectively (see Figure 6).[33] Other sharp absorptions are due to TBA ions.[34] Raman data (Figure

(33) Ryskin, Y. I. *The Infrared Spectra of Minerals*; Farmer, V. C., Ed.; Mineralogical Society: London, 1974.

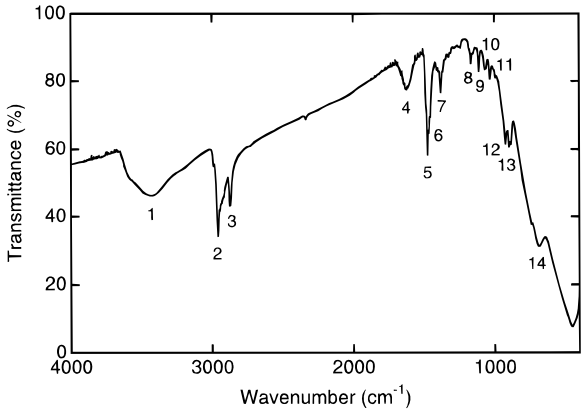

Figure 6. FT-IR spectra for the freeze-dried product: (1) 3440, (2) 2959, (3) 2873, (4) 1627, (5) 1485, (6) 1469, (7) 1381, (8) 1152, (9) 1108, (10) 1067, (11) 1030, (12) 920, (13) 890, (14) 687 cm^{-1}.

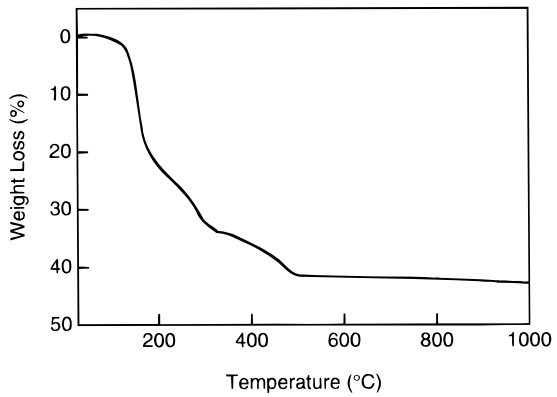

Figure 7. Thermogravimetric curve for the freeze-dried gel.

4b) were accounted for by a superposition of bands from the host framework and those from TBA ions.

The final step of the synthesis (step III) involves transformation of the TBA intercalated gel to titanium dioxide by heating. As shown in Figure 7, the gel lost considerable weight up to 500 °C.[35] Liberation of interlayer TBA ions and H_2O molecules is responsible for the mass loss, the magnitude (~40%) of which is consistent with the chemical formula above. The lamellar structure was destroyed due to the removal of the interlayer species and titanium dioxide started to be crystallized as anatase above 350 °C as exemplified by XRD data shown in Figure 2d,e. Raman data also provided clear evidence for this crystallization scheme (Figure 4c,d). The bands for TBA ions and the layered host disappeared and the intense bands emerged instead at 142, 395, 515, and 636 cm^{-1}, which are diagnostic for anatase.[36] The overall microscopic texture as well as the spongy appearance remained substantially unchanged during the heat treatment. As a consequence, the thin flakes of titanium dioxide were obtained as the final product.

The flaky morphology is visualized in Figure 3c,d. The individual flakes are characterized by their high aspect ratio as well as their thinness, i.e., tens nanometers in thickness versus micrometers in lateral size. This shape renders excellent slipping or extensible properties to the material, which may facilitate efficient coating of some surface in a thin layer.

Table 1. Textural Characteristics

	heat-treated temp (°C)		
	350	500	700
specific surface area ($m^2\ g^{-1}$)	104	74	47
specific pore volume ($cm^3\ g^{-1}$)	0.264	0.312	0.257
mode pore size (nm)	23	31	23, 51

The flake surface became uneven upon heating (compare Figure 3b with c and d). The roughness became pronounced with increase of the heating temperature and, in an extreme case, the flakes developed holes. This change is attributable to crystallization/grain growth of titanium dioxide in the flakes, which can be followed by TEM more unambiguously. Figure 8 shows the micrograph for the flaky oxide prepared at 700 °C. The flakes apparently comprised small grains which can be identified as anatase on the basis of the electron diffraction data. A random orientation of individual grains over the entire flake was suggested from the concentric diffraction rings. The dimension (20−30 nm) was approximately equal to the crystallite size deduced from XRD line width of the 101 reflection for anatase. As depicted in Figure 9, the grain grew in size as the heating temperature increased, which may promote the formation of the unevenness. Consequently, it is concluded that the flake is polycrystalline, being built up from fine grains of anatase which are interconnected with each other in a quasi-two-dimensional manner.

Surface Characteristics. One of the noteworthy features for the material is related to the state of aggregation of the thin flakes. They were assembled in a very irregular and open manner. As expected from the texture, the material was porous. The typical N_2 gas adsorption/desorption isotherms are plotted in Figure 10. It is categorized as a type IV isotherm with a type H3 hysteresis according to IUPAC classification.[37] Textural parameters derived from the isotherm data are summarized in Table 1. Considerable enhancement of BET surface area was achieved by the synthetic approach presented here; note an original value of 1.5 $m^2\ g^{-1}$ for the parent protonic oxide, $H_xTi_{2-x/4}\square_{x/4}O_4 \cdot H_2O$.

The pore-size distribution curves revealed a wide distribution ranging from meso- to macropores (see Figure 11). The distribution was dependent on the heat-treatment as the final step of the synthetic process. Macropores tended to develop while a smaller portion of mesopores disappeared as the heating temperature raised. The thermal evolution of the pores suggests that the material contains three types of pore; (i) a smaller portion of mesopores, (ii) larger mesopores, and (iii) macropores, although they cannot be divided explicitly.

The first type of pores may be ascribed to internal cracks in the flakes. As mentioned above, the flake was constructed by fine grains of ~20 nm in diameter. Spherical particles of anatase of this dimension should have an external surface area of 37.8 $m^2\ g^{-1}$. The experimentally determined surface areas were higher than the calculated value, regardless of the fact that the grains were agglomerated with each other to form

(34) Absorptions at 3000−2800 and 1500−1370 cm^{-1} are assignable to stretching and bending vibrations of $-CH_3$ and $-CH_2-$ groups in alkyl chains, respectively. IR bands at 1152 cm^{-1} may be due to the C−N stretching mode.[43] Although full assignment cannot be made, the absorption frequencies were superimposable to the data for TBACl which was recorded for a reference purpose.

(35) A static heating completed the weight loss up to 400 °C.

(36) Cai, Y.; Ozkan, U. S. *Appl. Catal.* **1991**, *78*, 241.

(37) Sing, K. S. W.; Everett, D. H.; Haul, R. A. W.; Moscou, L.; Pierotti, R. A.; Rouquérol, J.; Siemieniewska, T. *Pure Appl. Chem.* **1985**, *57*, 603.

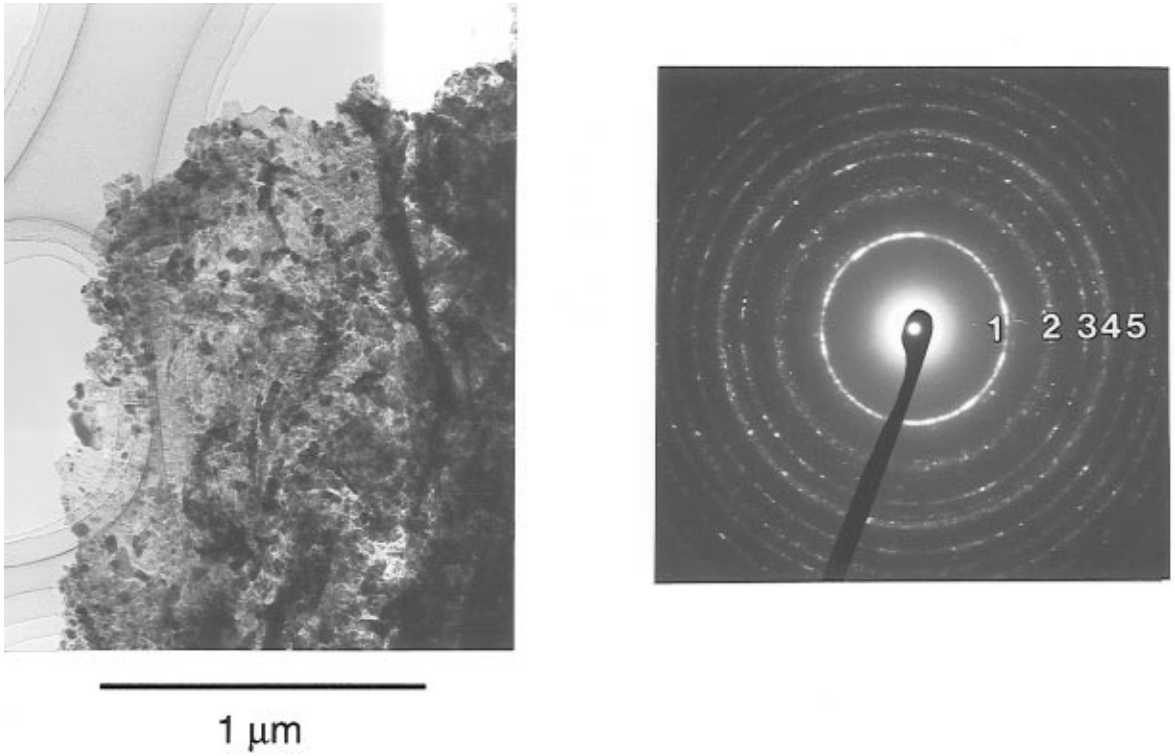

Figure 8. Transmission electron micrograph and electron diffraction pattern for the titanium dioxide thin flakes prepared at 700 °C. The diffraction rings are indexed as (1) 101, (2) 103 + 004 + 112, (3) 200, (4) 105 + 211, and (5) 213 + 204 for anatase.[44]

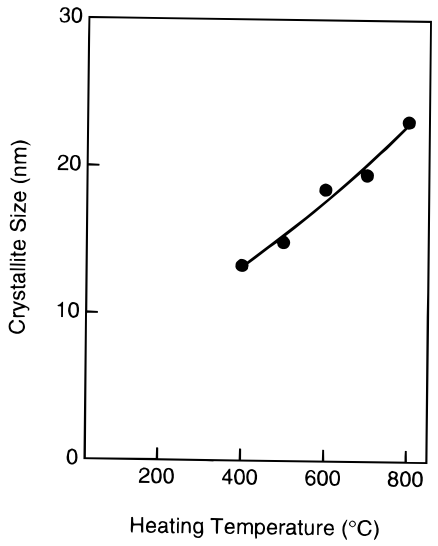

Figure 9. Crystallite size of anatase as a function of the heat-treated temperature.

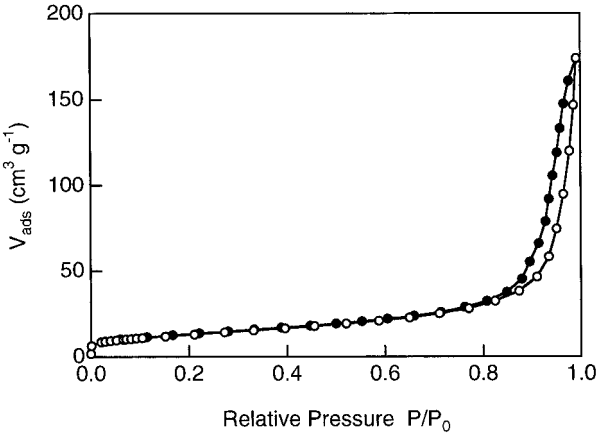

Figure 10. N_2 gas adsorption/desorption isotherms for the titanium dioxide thin-flake aggregate prepared at 700 °C. Open and closed circles express adsorption and desorption branches, respectively.

the flakes. This suggests the presence of internal pores especially in the materials prepared at lower temperatures. The appreciable drop in surface area by heating is most likely attributable to destruction of the internal pores. Similar phenomena have been widely observed for various porous materials.

The second type comprises a majority of pores in the material. Accordingly it predominantly governed the adsorption/desorption properties. Opening between the randomly assembled flakes may account for the second type pore structure. The observed hysteresis loop of type H3 is, as a rule, interpreted in terms of slit-shaped pores.[37] This is in agreement with the textural feature of the thin-flaky-particle aggregate of titanium dioxide.

The formation of the macropores appears to be associated with the degree of the unevenness on the flake surface. As mentioned above, the surface roughness was parallel to the heat-treatment temperature. This strongly suggests that the cavities on the surface may also serve as pores.

Porous titanium dioxide is of increasing interest principally due to potential for catalytic applications. Most of the synthetic approaches are based on sol−gel processes starting from titanium alkoxides.[38,39] Titanium dioxide xerogels, which are prepared by conventional drying, are mostly microporous.[38] On the other hand, supercritical drying results in materials of high surface area and high porosity, which are termed aerogels. It has been reported that their pore size can

(38) (a) Xu, Q.; Anderson, M. A. *J. Mater. Res.* **1991**, *6*, 1073. (b) Bischoff, B. L.; Anderson, M. A. *Chem. Mater.* **1995**, *7*, 1772.

(39) (a) Teichner, S. J.; Nicolaon, G. A.; Vicarini, M. A.; Gardes, G. E. E. *Adv. Colloid Interface Sci.* **1976**, *5*, 245. (b) Schneider, M.; Baiker, A. *J. Mater. Chem.* **1992**, *2*, 587. (c) Campbell, L. K.; Na, B. K.; Ko, E. I. *Chem. Mater.* **1992**, *4*, 1329. (d) Suh, D. J.; Park, T.-J. *Chem. Mater.* **1996**, *8*, 509.

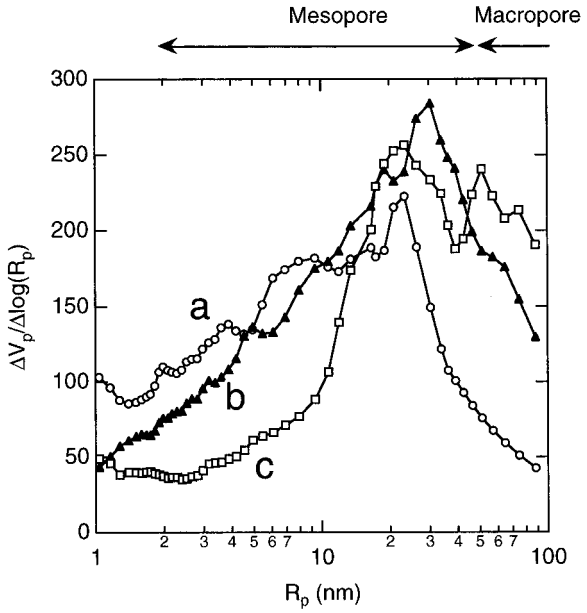

Figure 11. Pore-size distribution curves for the titanium dioxide thin flakes prepared at different temperatures: (a) 350, (b) 500, and (c) 700 °C. The range of meso- and macropores follows IUPAC definitions.[37]

be controlled in the range 10−30 nm.[39] Although the mesoporosity characteristics for the aerogels and the porous aggregate in the present study are apparently similar, they are distinguishable in terms of the geometrical shape of the pores. The aggregate of the flakes is characterized by its slit-shaped pores while the aerogels are by pores associated with polymeric networks. This difference reflects to the shape of the hysteresis loop of the isotherms.[40]

There have been few reports on preparation of porous aggregates of thin platelike particles except for several examples from clay minerals such as smectites.[41] Their porous aggregates have been synthesized by freeze-drying or supercritical drying of pillared or delaminated clay minerals. It has been reported that such porous structures catalyze various chemical reactions.[41a] The porous aggregate prepared in this study is of importance since it is constituted of titanium dioxide which itself exhibits high catalytic activities.

Catalytic Properties. Figure 12 shows the change in concentration of trichloroethylene as a function of UV irradiation time. A catalyst-free experiment showed some decrease (14% loss after 60 min), which may be due to the loss of the volatile chemical on its sampling for analysis. Without illumination, the flaky oxide hardly had influence on the decay of the reactant, showing a negligible departure from the blank test. In contrast, significant enhancement was observed when the dispersed system was irradiated by UV rays, which can be taken as photocatalytic degradation. The reaction proceeded in an apparently first-order fashion. Pruden and Ollis have studied the photoassisted decomposition of aqueous trichloroethylene using Fisher Certified grade titanium dioxide and showed a similar first-order decay.[42]

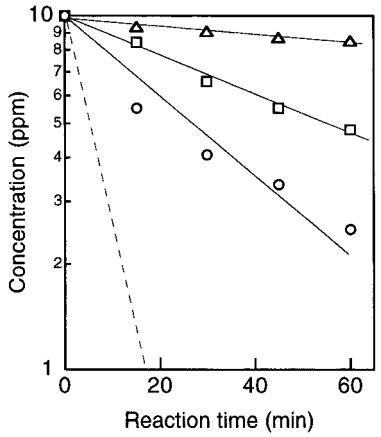

Figure 12. Photocatalytic degradation of trichloroethylene. Open and square symbols denote the data for the material prepared at 500 and 700 °C, respectively. Blank data are plotted by triangles. Dashed line denotes the data for Degussa P25 under the identical conditions.

The porous aggregate prepared at 700 °C exhibited a higher rate constant than the sample at 500 °C did. It is also noted that the catalytic activity was moderate in comparison with the data for Degussa P-25, one of the most active photocatalytic titanium dioxides, as shown by a dashed line in Figure 12. These differences may be correlated with a number of factors such as crystallinity of anatase, residual carbon content, and so on. Further study is required to obtain deeper and full understanding for the photocatalytic properties of the porous aggregate of the flaky titanium dioxide.

Conclusions

The titanium dioxide flakes tens nanometers thick were prepared by exfoliating the layered protonic titanate followed by freeze-drying and subsequent heating. The thin flakes were assembled into meso- to macroporous aggregates which were characterized by slit-shaped pores.

There are a number of layered hosts of diverse compositions and architectures. The synthetic strategy described in the present paper may provide approach for the design of these and their related materials in thin flaky forms and as a porous aggregate, which may widen the scope of their applications.

Acknowledgment. The authors wish to thank Messrs. M. Tsutsumi and Y. Kitami (National Institute for Research in Inorganic Materials) for their assistance in obtaining micrographs and Dr. T. Mori (Tosoh Corp.) for his discussion on the photocatalytic data.

CM9604322

(40) In general, the aerogels exhibit a type H2 loop while the porous material in this study did the type H3 one.

(41) (a) Pinnavaia, T. J.; Tzou, M.-S.; Landau, S. D.; Raythatha, R. H. *J. Mol. Catal.* **1984**, *27*, 195. (b) Lewis, R. M.; Kuroda, H. *Solid State Ionics* **1989**, *32/33*, 373. (c) Takahama, K.; Yokoyama, M.; Hirao, S.; Yamanaka, S.; Hattori, M. *J. Mater. Sci.* **1992**, *27*, 1297.

(42) Pruden, A. L.; Ollis, D. F. *J. Catal.* **1983**, *82*, 404.

(43) *Handbook of Chemistry and Physics*; Weast, R. C., Ed.; CRC Press: Cleveland, 1974.

(44) Reflections 2, 4 and 5 were not well-resolved due to low crystallinity.